ADAPTIVE WAVELENGTH SCANNING LIDAR (AWSL) FOR 3D MAPPING FROM SPACE

Guangning Yang, David J. Harding, Jeffrey R. Chen, Mark A. Stephen, Xiaoli Sun, Hui Li, Wei Lu, David R. Durachka, Zoran Kahri, Kenji Numata, Xiaozhen Xu, Erwan Mazarico, Kenneth J. Ranson, Philip W. Dabney, James Mackinnon and Travis W. Wise

All at: NASA Goddard Space Flight Center, 8800 Greenbelt Rd, Greenbelt, MD 20771, USA
Email: guangningyang-1@nasa.gov

ABSTRACT

We present the design and performance of an adaptive wavelength scanning lidar (AWSL) for highly efficient mapping from low Earth orbit (LEO). Mapping is accomplished by steering a laser beam across 1,200 resolvable spots using wavelength tuning and grating dispersion. Any subset of these 1,200 spots can be selected by wavelength switching. The design is validated with an 1550-nm prototype using a fast wavelength-tuned (500-kHz) pulsed (2-ns) fiber laser with the beam dispersed by gratings for beam steering. Reflected pulses are detected with an eight-pixel detector array with single-photon sensitivity. Eight lidar returns are time-multiplexed to one output that is digitized with a single 1-GSPS-digitizer, to save power. A grating spectrometer rejects solar background noise spatially and spectrally, and images laser footprints on to the detector array. The gratings retain the fiber laser beam quality. We are developing a 1030-nm AWSL intended for a LEO SmallSat platform.

***Index Terms*—** ranging lidar, adaptive lidar, laser altimeter, imaging lidar, wavelength scanning

1. INTRODUCTION

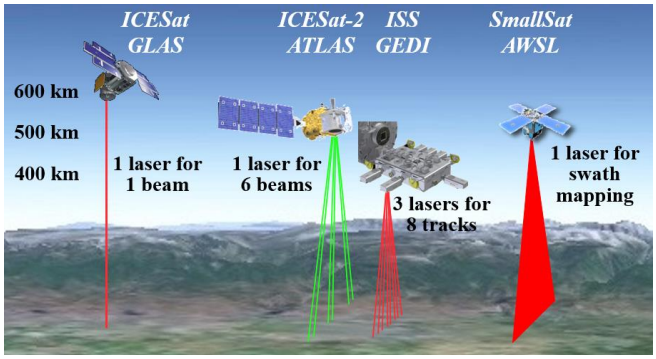

Figure 1. The progress of NASA Earth science altimetry lidar missions, from single-beam GLAS to multiple-beam ATLAS and GEDI. AWSL provides a low SWaP path to spaceflight 3D mapping.

Spaceborne laser altimeters provide high precision global elevation data needed for determining changes in ice sheet heights, sea ice thickness, vegetation structure and land topography as well as for atmospheric cloud and aerosol profiling. NASA has launched three Earth orbiting laser altimeter instruments in the past twenty years (Figure 1). The first was the Geoscience Laser Altimeter System (GLAS) on the NASA Ice, Cloud and land Elevation Satellite (ICESat) [1], operated from 2003 to 2009. GLAS is a single-beam pulsed laser altimeter operating at 40-Hz and the return analog waveform is digitized. The second launched instrument is the Advanced Topographic Laser Altimeter System (ATLAS) on the NASA ICESat-2 mission [2]. It employs a micro-pulse laser operating at 10-kHz pulse rate. The laser beam is passively split into three pairs of beams, where each pair has a weak and a strong beam. The receiver operates in photon counting mode. The ATLAS/ICESat-2 instrument has been operating in space since 2018. The most recent laser altimeter is the Global Ecosystem Dynamics Investigation (GEDI) [3]. It was launched in late 2018 and operates from the International Space Station (ISS). It has three solid-state pulsed lasers, each operating at 241-Hz. The beams are split and optically dithered to form eight ground tracks. Both GLAS and GEDI employ 1064-nm Q-switched solid-state pulsed lasers and detected waveforms from digitized silicon avalanche photodiode (APD) detectors. Their laser pulse rates are low because the relatively low sensitivity of the Si APD detector requires large pulse energy. ATLAS uses a 532-nm micro-pulse solid-state laser at a much higher pulse rate (10-kHz) and high-sensitivity PMT photon-counting detectors that can detect much lower energy laser pulses. To cover more tracks on the surface, two approaches have been adopted for the space missions: 1) increasing the number of lasers (GEDI) and 2) splitting a laser beam to illuminate several tracks (both ATLAS and GEDI). However, more lasers means increased size, weight and power (SWaP,) and splitting the laser beam requires higher laser pulse energy.

Compared to these three profiling missions, recommendations in the 2017 National Academies Earth Science Decadal Survey for future laser altimetry observations require significantly greater coverage for ice sheets and sea ice (Ice Elevation Observable, IE) and 3D height mapping for vegetation structure and topography (Terrestrial Ecosystem Structure TES, and Surface Topography and Vegetation STV Observables) [4]. Global

sampling for IE and TES were recommended to be done as moderate cost Explorer missions ($350M cap) this decade and global mapping for STV to be done next decade.

There is therefore a great need to drastically improve lidar SWaP efficiency to enable more coverage and use of smaller, cost-effective satellite platforms. This calls for: 1) the optimized receiver performance with single-photon sensitivity; 2) higher laser wall-plug efficiency; 3) sufficient laser pulse peak power for shot-noise limited receiver performance; 4) full waveform digitization, rather than single photon counting, to improve performance; and 5) innovative receiver electronics to efficiently handle the vast numbers of high-speed lidar return channels. Our AWSL approach addresses these aspects with patent-pending designs and state-of-the-art transmitter and receiver technologies.

2. AWSL ARCHITECTURE DESIGN AND PERFORMANCES

2.1. AWSL instrumentation

Figure 2 depicts the architecture of the AWSL system, illustrating cross-track wavelength-to-angle scanning, imaging of the return pulses onto a detector array, and multiplexing electronics.

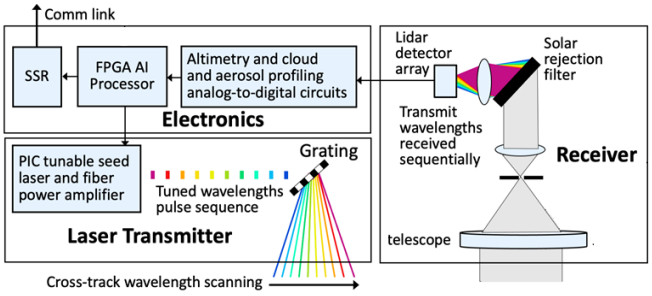

Figure 2. AWSL lidar system block diagram with three major blocks: laser transmitter, receiver, and electronics (see text for details).

2.2.1. AWSL Transmitter

The laser transmitter employs a photonic integrated circuit (PIC) based fast-wavelength-tuning pulsed laser, a high peak power fiber amplifier, and a transmitter telescope with dispersive gratings to map wavelengths to angles corresponding to distinct lidar footprints on the surface. A 1030-nm laser transmitter with a 30-nm tuning range can scan 1,200 resolvable spots cross-track over an angular range of 0.825deg, corresponding to 7.2-km from a 500-km orbit. Any subset of these 1,200 spots can be scanned by wavelength switching. Beam-steering rather than beam-splitting decreases the laser pulse energy requirement, while still enabling high-precision measurements on each ground track. The laser can operate up to several hundred kHz, enabling dense measurements of the Earth's surface.

2.2.2. AWSL Receiver

The return pulses are collected by a receiver telescope. The solar background radiation for each individual footprint is filtered spatially and spectrally by a grating spectrometer that images the surface footprints onto a linear APD detector array. The optical bandpass filter design has 0.6-nm bandwidth for each footprint. A state-of-the-art Mercury Cadmium Teluride (HgCdTe) APD detector array [5] is used for the receiver. It operates in linear mode with single-photon sensitivity and allows multiple photons to be detected simultaneously to overcome solar background and detector dark noise.

2.2.3. Electronics

Lidar return waveforms are digitized to allow better performance than binary thresholding of the return pulses. The electronics incorporates a RF-multiplexer that time-multiplexes multiple lidar-returns into a single output (8-to-1). Only one digitizer (1-GSPS) is used for each multiplexer output to digitize signals from eight tracks. A field-programmable gate array (FPGA) is used to process the digitized data and the processed data are stored in a solid-state recorder (SSR). Time-multiplexing the return signals dramatically reduces the SWaP of the electronics.

2.2. AWSL design

The AWSL can be designed to operate at various center wavelengths. For our Earth science application, 1030-nm is chosen because it offers the best overall trade in a range of performance metrics: 1) the surface reflectance at 1-μm is much higher for vegetation than at 0.5-μm and for snow and ice than at 1.5-μm; 2) solar irradiance background and atmospheric transmission are more favorable at 1-μm than at 0.5-μm; and 3) the Yb-doped fiber amplifier (YDFA) at 1.03-μm is much more efficient than the Er-doped fiber amplifier (EDFA) at 1.5-μm.

Table 1. Eight-channel AWSL performance parameters

Parameter	Value	Unit
Center wavelength	1550	nm
Wavelength tuning range	32	nm
Wavelength tuning rate	500	kHz
Resolvable Spots	579	
Transmitter pulse width	2	ns
Transmitter pulse peak power	700	W
Number of wavelengths per sweep	8	
Per wavelength tuning rate	8	kHz
FWHM of optical filter passband	0.6	nm
Detector excess noise factor	1.1	
Detector noise equivalent power	0.3	fW/sqrtHz

For the 1030-nm AWSL, several key technologies are still in development, especially the 1030-nm fast wavelength tuning laser. Starting with a mature 1550-nm tunable laser we

built a bench-top technology demonstration system with 32-nm tuning range. The key design parameters are listed in Table 1.

2.3. AWSL 1550-nm performance

We have used the 1550-nm system to validate all key performance parameters during laboratory testing: fast wavelength tuning, wavelength-to-angle conversion, beam quality of the transmitted laser, transmitter and receiver transmittance, all-wavelength filtering, beam quality of received pulses at the detector focal plane, electronic time-multiplexing, high speed digitizing, and restoration of precision laser pulse time-of-flight (ToF) by referencing back to the start pulses. The bench top system consists of an optical assembly and an electronics PXI-chassis. One side of the optical assembly hosts the transmitter telescope followed by two orthogonally oriented gratings. The first grating accomplishes the wavelength-to-angle scanning and the second is inserted to flatten the scanning "smile" of the footprint images on the detector focal plane. The other side of the optical assembly hosts the receiver telescope, the grating spectrometer, and the single-photon-sensitive HgCdTe APD array. The PXI-chassis electronics box includes a fast wavelength tuning laser, a 2ns pulse generator, fiber pre- and power- amplifiers, RF-multiplexer, a FPGA module (with high speed digitizers) for digitization, timing, data acquisition, data processing, and a host computer for overall instrument operation. The instrument is configured to operate with a total of eight wavelengths per sweep (limited by the detector array size) with the sweep repeated at 8-kHz rate (Figure 3). The sweep yields an 8-kHz pulse rate per detector pixel, necessary to prevent unwanted cloud folding when operating from orbit.

a. Laser pulse train | b. Laser spectrum

Figure 3. The transmitted laser pulse train and the optical spectrum.

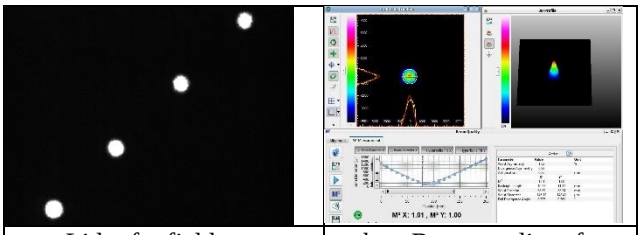

a. Lidar far field spots. | b. Beam quality of transmitted lidar beam.

Figure 4. Four of eight lidar far field spots (measured with a 1-meter focal length lens and an infrared camera) and transmitted laser beam quality measured with a m-squared meter.

2.3.1. Laser transmitter performance

The eight wavelengths per sweep are 82-GHz apart and the total wavelength step rate is 64-kHz. At this fast wavelength step rate, our laser maintains a wavelength stability better than 1-GHz and >40-dB side mode suppression for each individual wavelength. A 2-ns laser pulse is synchronously carved for each wavelength step. An EDFA boosts the pulse peak power to 700-W (sufficient for our planned ground-based tests at up to 3-km range) with an on/off power extinction ratio of 30-dB. To measure the angular separation of the beam spots, the transmitted laser beam is focused by a 1-meter focal length lens onto an infrared camera. Figure 4a shows the laser spots of the central 4 wavelengths. The dispersion power was calculated based on the focal length and camera pixel size. The measured result matches the design value. The laser beam quality is measured to be $M^2(x) = 1.01$ and $M^2(y) = 1.00$, as shown in Figure 4b. This indicates that the gratings retain the single-mode laser beam quality. Transmitter power meter measurements documented an optical path transmittance of 90%.

2.3.2. Receiver performance

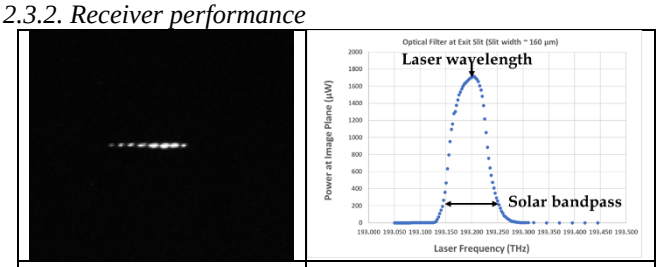

a. Lidar spot images on the detctor. | b. Spectrum of all-wavelength filter for each wavelength

Figure 5. lidar footprint images on the detector focal plane and the spectrum of the all-wavelength filter.

The transmitted laser beam is looped back to the receiver with a retroreflector to simulate the lidar far-field returns. The eight wavelength spots are imaged onto the detector array. Figure 5a shows the lidar spots imaged onto the detector focal plane. The spot-spacing matches the detector pixel pitch of 64-µm. Although the optical power for each spot (measured at the detector focal plane) is quite close to each other, the brightness of the spots on the infrared camera is uneven due to the camera's non-flat spectral response.

The beam quality of the laser beam after passing the receiver grating is measured to be $M^2(x) = 1.08$, $M^2(y) = 1.04$. This indicates our receiving optics (including the grating) essentially retains the single-mode beam quality. The FWHM bandwidth of the all-wavelength-filter is measured to be 0.6-nm, matching the design value. Receiver power

measurements documented an optical path transmittance of 84%.

2.3.3. Electronics performance

The eight detector outputs are time-multiplexed into a single output, which is subsequently digitized with a 1-GSPS digitizer (Figure 6). The corresponding start pulses are digitized with a separate digitizer. The ToF of each pulse is calculated referencing the corresponding start pulse. The results are shown in Figure 7 for all eight spots. This validates our time-domain multiplexing design that dramatically reduces the receiver SWaP.

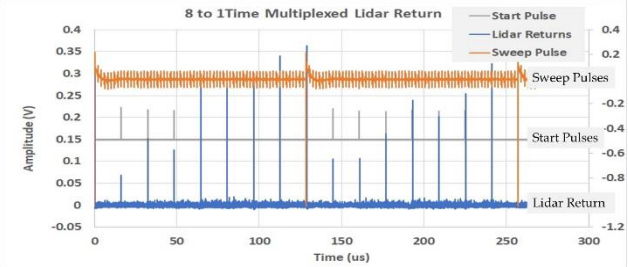

Figure 6. multiplexed electrical signals of the start and received laser pulses, to be digitized by two 1PPS digitizers.

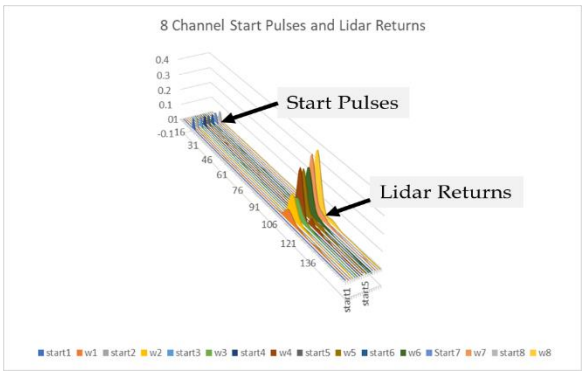

Figure 7. Demultiplexed electrical signals where each received pulse is referenced to its own start pulse for ToF computation.

3. CONCLUSION AND FUTURE WORK

An AWSL system operating at 1550nm was designed, built and evaluated by laboratory testing. All key performance parameters and operation concepts of AWSL were validated with this prototype system. This includes fast laser wavelength steps at rates up to 500-kHz with 2-ns synchronized pulse modulation. The laser achieved 40-dB side-mode suppression, 30-dB pulse modulation extinction ratio, and 700-W pulse peak power. The gratings do not degrade the laser beam quality and transmittance through the transmitter optical path is 90%. The grating-based imaging spectrometer provides excellent spatial and spectral rejection of solar background and the transmittance through the receiver optical path is 84%. Eight wavelength-scanned spots were directly mapped to a single-photon-sensitive HgCdTe APD detector array. These eight lidar returns are waveform digitized with a single 1-GHz digitizer after 8-to-1 time-domain multiplexing. The time-of-flight of each spot is calculated by referencing each return to its own start pulse. The operation and performance of the 1550-nm prototype AWSL is fully validated.

We plan to perform horizontal path ranging experiments with this prototype system on natural targets within 3-km range in the coming months to validate our lidar link performance model used for spaceflight instrument design purposes. We are also developing a 1030-nm AWSL system targeting a low-earth-orbit SmallSat platform to meet Earth Science Decadal Survey recommendations. Limited by available power and detector array size, it will be able to image a swath in 3D up to 1.5km wide and distribute profiles emulating ICESat-2 and GEDI across 7.2km. The flexibility enabled by our high-pulse-rate, low SWaP AWSL approach can also be tailored to a wide range of applications for planetary science objectives, and autonomous navigation and landing.

4. REFERENCES

[1] B. E. Schultz, H. J. Zwally, C. A. Shuman, et al., "Overview of the ICESat Mission," Geophysical research letters, Volume 32, Issue 21, (2005).

[2] T. Markus, T. Neumann, A. Martino, et al., "The Ice, Cloud, and land Elevation Satellite-2 (ICESat-2): Science requirements, concept, and implementation," Remote sensing of environment, Volume 190, (2017).

[3] R. Dubayah, J. B. Blair, S. Goetz, et al., "The Global Ecosystem Dynamics Investigation: High-resolution laser ranging of the Earth's forests and topography," Science of Remote Sensing, Volume 1 (2020).

[4] Committee on the Decadal Survey for Earth Science and Applications from Space, "Thriving on Our Changing Planet: A Decadal Strategy for Earth Observation from Space", National Academies of Sciences, Engineering, and Medicine, 700 pp, (2017).

[5] X. Sun, J. B. Abshire, M. A. Krainak, W. Lu, J. D. Beck, et al., "HgCdTe avalanche photodiode array detectors with single photon sensitivity and integrated detector cooler assemblies for space lidar applications," Optical Engineering, 58(6) 067103 (2019).

5. ACKNOLOGYMENTS

This work was funded/supported by:
1. NASA ESTO funding IIP-19-0052
2. NASA GSFC "RI2 Cross Cutting Technology"
3. NASA GSFC "IRAD Communication and Navigation"
4. NASA GSFC Earth Science Line of Business
5. NASA GSFC Planetary Science Line of Business
6. NASA STMD Precision Landing